Electrical Power and Energy Systems 116 (2020) 105525

Contents lists available at ScienceDirect

Electrical Power and Energy Systems

journal homepage: www.elsevier.com/locate/ijepes

Environmental economic dispatch of integrated regional energy system considering integrated demand response

Liangce He[a], Zhigang Lu[a,*], Lijun Geng[a], Jiangfeng Zhang[b], Xueping Li[a], Xiaoqiang Guo[a]

[a] Key Lab of Power Electronics for Energy Conservation and Motor Drive of Hebei Province, Yanshan University, Qinhuangdao, Hebei 066004, China
[b] School of Electrical and Data Engineering, University of Technology Sydney, Ultimo, NSW 2007, Australia

ARTICLE INFO

Keywords:
Integrated regional energy system
Environmental economic dispatch
Energy hub
Integrated demand response

ABSTRACT

To reduce the emissions of greenhouse gases and air pollutants, various low-emission measures have been taken in the power system, which are gradually intensifying the interdependency among different energy systems. Considering the carbon trading scheme and different air pollutant control technologies, this paper proposes an environmental economic dispatch model for the coordinated operation of an integrated regional energy system, which consists of a regional electricity supply network and a natural gas network, along with district energy hubs. Each energy hub contains a combined heat and power unit, a CO_2-capture-based power to gas facility, a heat pump, a gas furnace and different energy storage facilities. To achieve an optimized balance between operational cost and emissions during the environmental economic dispatch of this integrated regional energy system, a price-based integrated demand response program is introduced in the energy hub. Then the proposed model is converted into a mixed-integer linear programming problem to find solutions efficiently. Case studies are carried out to demonstrate the effectiveness of proposed environmental economic dispatch model of the integrated regional energy system.

1. Introduction

Threatened by global warming and air pollution, environmental issues have caught increasing attention in recent years. In 2015, the Paris Agreement sets up the target to keep the increase of global temperature well below 2 Celsius degrees above pre-industrial levels [1]. Additionally, a series of detailed provisions have been implemented by many countries to reduce the pollution emissions [2].

Nowadays, the power system mainly depends on fossil fuel power plants, which are one of the major emission sources of greenhouse gases and air pollutants, and thus various measures have been taken to mitigate their environment impacts. Firstly, gas-fired units and combined heat and power (CHP) units are widely built, due to their lower pollutions and higher energy efficiencies [3]. Secondly, different emission control technologies are developed for fossil fuel power plants. For instance, carbon capture and storage (CCS) technologies can effectively reduce CO_2 emission [4], while the selective catalytic reduction (SCR) technology and the flue gas desulfurization (FGD) technology can be separately deployed to reduce the emissions of NO_x and SO_2 [5]. Thirdly, large-scale renewable energy sources are gradually integrated into the power system, especially wind and solar power. The Global Wind Energy Council forecasts that the newly installed capacity of wind power will be at least 55 GW each year until 2023 [6]. To deal with the intermittency of wind power output, diversity flexibility options [7], such as power to gas (P2G) technology and demand response (DR) programs, are developed to improve the wind power utilization.

The traditional environmental economic dispatch (EED) problem is to optimize both economic cost and environmental cost with operational constraints of the power system [8]. However, these power system constraints will not be sufficient to describe integrated energy systems where CHP units and gas-fired units appear in the interconnected electrical power system, district heating network and natural gas supply network. With the continuing increase of the installed capacity of gas-fired units, P2G facilities and CHP units, the interdependence of electricity network, natural gas network and district heating network is increasingly intensified, which calls for the relevant research on these integrated energy systems (IES) [9]. In the context of IES, if the EED only considers the operational constraints of the power system, it will result in sub-optimal or even infeasible operation for other energy systems. Therefore, it is of great significance to study the EED considering the operational constraints of the overall IES.

There are already existing studies on the EED of IES. To reduce the CO_2 emission, a stochastic security-constrained unit commitment model is proposed in [10] under the CO_2 emission limit and operation

* Corresponding author.
E-mail address: zhglu@ysu.edu.cn (Z. Lu).

https://doi.org/10.1016/j.ijepes.2019.105525
Received 6 May 2019; Received in revised form 22 August 2019; Accepted 1 September 2019
Available online 11 September 2019
0142-0615/

Nomenclature

Indices and sets

b, n	indices of electricity network buses and gas network nodes
c, $c1$, $c2$	indices of compressors, compressor head nodes, and compressor tail nodes
d	index of load demand
e, g, h	indices of electricity, gas, and heat
i, j, k, w	indices of coal-fired units, gas-fired units, energy hubs, and wind farms
l, $l1$, $l2$	indices of transmission lines, line head buses, and line tail buses
p, $p1$, $p2$	indices of gas pipelines, pipeline head nodes, and pipeline tail nodes
t,τ	indices of hours
ω	indices of gas wells
Ω_{E}, Ω_{EH}	sets of energy carriers and energy hubs
Ω_{B}, Ω_{N}, Ω_{TL}	sets of electrical buses, gas network nodes, and transmission lines
Ω_{CU}, Ω_{GU}, Ω_{WF}	sets of coal-fired units, gas-fired units, and wind farms
Ω_{COM}, Ω_{GP}, Ω_{PP}, Ω_{WE}	sets of gas compressors, gas pipelines, passive pipelines, and gas wells

Variables

$ES_{(\cdot),kt}$	storage capacity of storage facility in energy hub k at time t
$I^{\mathrm{in}}_{(\cdot),kt}$, $I^{\mathrm{out}}_{(\cdot),kt}$	statuses for inflow/outflow of storage facility in energy hub k at time t
$I_{\mathrm{PtG},kt}$	status indicator of power to gas facility in energy hub k at time t
L_{dt}	load demand d at time t
P_{it}, P_{jt}, P_{wt}	power outputs of coal-fired unit i, gas-fired unit j, and wind farm w at time t
PL_{lt}	power flow of transmission line l at time t
Pr_{nt}	pressure of gas node n at time t
$Q^{\mathrm{CO_2}}_{(\cdot)}$, $Q^{\mathrm{CO_2}}_{\mathrm{R},(\cdot)}$	CO_2 emission/emission quota
Q_{jt}	gas consumption of gas-fired unit j at time t
$Q^{\mathrm{NO_x}}_{(\cdot)}$	NOx emission
Q_{pt}	gas flow of gas pipeline p at time t
$Q_{\omega t}$	gas production of gas well ω at time t
$S_{(\cdot)}$, $S^{\mathrm{in}}_{(\cdot)}$, $S^{\mathrm{out}}_{(\cdot)}$	state variables of energy hub
$\theta_{(\cdot)}$	bus voltage angle
ρ_{dt}	price of load demand d at time t

Constants

$a_{(\cdot)}$, $b_{(\cdot)}$, $c_{(\cdot)}$	heat rate curve coefficients
$A_{b(\cdot)}$, $B_{n(\cdot)}$	incidence matrices for bus b and node n
C_p	gas flow coefficient of gas pipeline p
$E_{d,(\cdot)}$	price elasticity of load demand d
EL_{bt}, GL_{nt}, P^{f}_{wt}	forecast values of electricity load b, gas load n, and wind farm w at time t.
L^{ini}_{d}	initial value of load demand d
$RU_{(\cdot)}$, $RD_{(\cdot)}$	ramp up/down rate of a unit
$\alpha^{\mathrm{NO_x}}_{i}$, $\beta^{\mathrm{NO_x}}_{i}$, $\gamma^{\mathrm{NO_x}}_{i}$	NOx emission coefficients of coal-fired unit i
$\kappa^{\mathrm{NO_x}}_{(\cdot)}$, $\delta^{\mathrm{NO_x}}_{(\cdot)}$	NOx emission reduction coefficients for generating units with lower NOx burner and selective catalytic reduction device
$\eta_{(\cdot)}$	efficiencies of different facilities in energy hub
$\rho^{\mathrm{CO_2}}$, $\rho^{\mathrm{NO_x}}$	carbon trading price and NOx emission penalty price
ρ^{ini}_{d}	initial price of load demand d
ρ_{i}	generation cost of coal-fired unit i
ρ_{ω}	gas production cost of gas wellω
$\mu^{\mathrm{CO_2}}_{(\cdot)}$, $\chi^{\mathrm{CO_2}}_{(\cdot)}$	CO_2 emission/emission quota coefficients
$\mu^{\mathrm{NO_x}}_{\mathrm{L},j}$, $\mu^{\mathrm{NO_x}}_{\mathrm{D},j}$	NOx emission coefficients of gas-fired unit i
$\upsilon^{\mathrm{CO_2}}_{\mathrm{PtG},k}$	CO_2 reaction coefficient of power to gas facility in energy hub k
$\lambda^{\mathrm{NO_x}}_{(\cdot)}$	threshold coefficient of selective catalytic reduction device
$\varsigma^{\mathrm{NO_x}}_{j}$	combustion mode coefficient of combined cycle gas turbine j
ϕ^{l}_{d}, ϕ^{u}_{d}	acceptable price adjustment coefficients of load demand d
φ^{l}_{d}, φ^{u}_{d}	IDR participation coefficients of load demand d
$(\cdot)_{\mathrm{min\,/\,max}}$	min/max value of a quantity

constraints of electricity and natural gas infrastructures. A flexible operation mode of carbon capture systems and P2G facilities is analyzed in [11], and the CO_2 processing cost is considered in a low-carbon economic dispatch model of electricity-gas IES. In [12], CO_2 emission cost is embedded into an optimal energy flow model of electricity-gas-heat IES, and then the locational margin prices are calculated. In [13], an optimal energy flow model of large-scale IES is presented considering the carbon trading market, and three decentralized algorithms are adopted to deal with the limited information exchange of different subareas. In [14], the carbon emission flow theory is extended to the IES from the power system, and the corresponding calculation methods are proposed to quantify the carbon emission responsibility among different energy systems. Except for CO_2, the air pollutant emissions of SO_2 and NO_x have also been considered in [15], and an interval optimization strategy is proposed of electricity-gas IES. To better control the air pollutant concentration, a spatial and temporal diffusion model of air pollutant emissions is presented in [16], and a two-layer convex decentralized optimization is proposed to handle the information sharing difficulties between electricity and natural gas systems. However, mature air pollution control technologies, such as SCR and FGD, which have been widely deployed in existing fossil fired power plants, are not considered in [10–16].

Furthermore, demand response (DR) is one of the most effective means to reduce the EED costs of the power system [17,18], and various DR programs have been applied in the IES operation. The coupon-based DR and interruptible-load based DR are both integrated into virtual power plants to maximize the daily profit of an electricity-gas IES utility company [19]. Considering the load forecast errors and random outages of the power system, an hourly electricity DR is incorporated into the stochastic coordinated scheduling of electricity-gas IES to reduce the system operation cost by offering a flat load profile [20]. On this basis, an hourly gas DR is analogously formulated in [21] to relieve power shortage of gas-fired units, and the integrated gas-electricity DR programs are further discussed for their impact on the energy market clearing and locational marginal energy prices. Similarly, to coordinate the peak electricity and gas loads of electricity-gas IES, an incentive DR program is presented with compensation prices for different load nodes [22]. However, these DR programs in [19–22] may result in customers' discomfort due to modifying their desired load profiles to the scheduled patterns. A comprehensive review of the integrated demand response (IDR) is conducted in [23], which points out that the IDR can utilize the complementarity of different energy carriers to improve the operation characteristics of different IES while maintaining the customers' comfort. In [24], a stochastic scheduling model is proposed for interconnected EHs considering an IDR program, where the IDR program is divided into an internal DR program and an external DR program. The internal DR is achieved by the energy conversion process within the smart EH, while the time-shifting and interruptible DR programs are

defined as the external DR on the customer side. In [25], an IDR program with different energy storage devices is studied within the smart EHs, and a bi-level optimization model is formulated to reduce the operational cost of the electricity-gas-heat IES. Aiming to maximize the profit of natural gas and electricity utility companies and minimize the cost of customers simultaneously, a non-cooperative game model is proposed in [26] by embedding an IDR program into a set of smart energy hubs (EHs). However,

the above studies [19–26] mainly adopt various DR programs to improve the operation economy of different IESs, while the environment impacts have not been discussed.

In view of the above issues, this paper aims to study the EED for large scale IES, i.e., the integrated regional energy systems (IRESs), by considering the impact of air pollutant control technologies and DR programs. The concept of IRES is the same as what is called 'regional-district IES' in [27], and it contains key objects like the regional electricity and natural gas transmission networks, the loads, and the connections between the regional transmission networks and the loads, such as the distribution, conversion and storage facilities which can be well-described by the concept of EH.

The main contributions of this paper are listed in the following two aspects.

(1) An EED model is proposed for an IRES considering the operational cost and the emission cost simultaneously. To reduce the emissions of greenhouse gas CO_2 and air pollutant NOx, a carbon trading scheme is introduced, and different air pollution control technologies are deployed in the fossil-fired power plants.
(2) EHs are considered within the IRES, and each EH contains a CHP unit, a CO_2-capture-based P2G facility, a heat pump, a gas furnace and different energy storage facilities. Additionally, a price-based IDR program is embedded into these EHs to improve the EED of the IRES.

The remaining part of this paper is organized as follows. In Section 2, system descriptions of the IRES are presented, and the formulation of a price-based IDR is given. In Section 3, the gas emission models are introduced, and then the EED model of IRES is presented. Several case studies are analyzed in Section 4, and main conclusions are drawn in Section 5.

2. System description and integrated demand response

2.1. Description of IRES

The system sketch of an IRES is illustrated in Fig. 1. The energy transmission part of this IRES is composed of the electricity network and natural gas network, which are coupled by gas-fired power generation units and EHs. Each EH contains the electricity load and gas load of the IRES, power generation and energy storage facilities. Since its optimal management is considered here under IDR, it is also referred as a smart EH. Note that P2G and energy storage facilities can appear in both the regional energy transmission networks and the local EHs. To simplify the analysis, we assume that the P2G and energy storage facilities only appear in the EHs. Meanwhile, similar to many existing studies [11,12,21,22], we also assume that the presented IRES can be controlled by one utility to achieve the operation optimization.

2.2. EH

Energy hub is a novel concept to integrate multiple energy carriers. It is mainly composed of input ports, internal elements and output ports. The input ports are connected to the transmission or distribution networks of multiple energy systems as demand. Different energy demands at the output ports are supplied by three types of supplying elements, i.e., direct connection elements, energy conversion elements and energy storage elements. The structure of an EH is shown in Fig. 2.

The electricity P_e and natural gas P_g are supplied from the electricity network and natural gas network, respectively. The direct connection elements (a transformer or a gas pipeline), energy conversion elements (a CO_2-capture-based P2G facility [28], a CHP unit, a gas furnace and a heat pump), and energy storage elements (a heat storage or a gas storage) are coordinated to meet the consumers' electricity demand L_e, heat demand L_h, and gas demand L_g. To reduce the calculation complexity, the linear mathematical model of the EH is formulated by the state variables of internal elements [29]. For the direct connection elements and the energy conversion elements, the input variables are chosen as the state variables, i.e., S_T, S_G, S_{PtG}, S_{HP}, S_{CHP}, and S_{GF}.

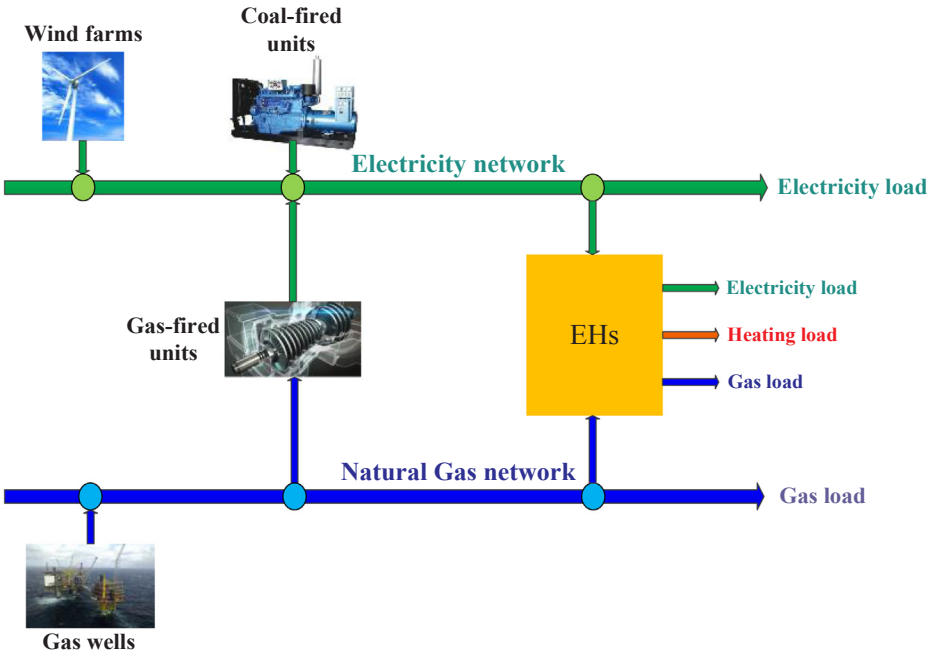

Fig. 1. Framework of an IRES.

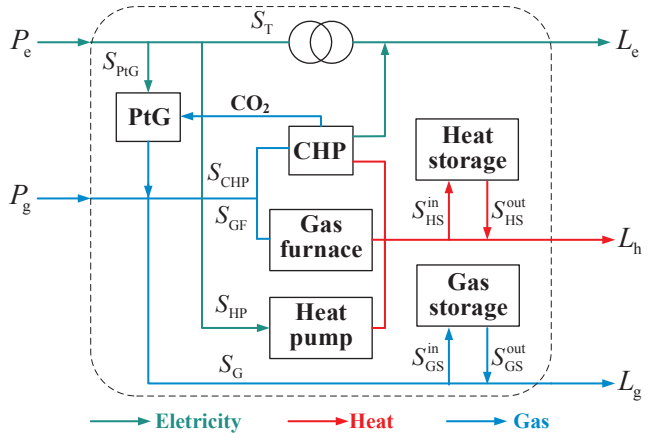

Fig. 2. Structure of an EH.

Additionally, the state variables for the energy storage elements are composed of both input variables and output variables, i.e., S^{in}_{HS}, S^{in}_{GS}, S^{out}_{HS}, and S^{out}_{GS}. With these state variables, the relationship between state variables and output port variables can be described as (1).

$$\begin{bmatrix} L_e \\ L_h \\ L_g \end{bmatrix} = \begin{bmatrix} \eta_{T,e} & 0 \\ 0 & 0 \\ 0 & 1 \end{bmatrix} \begin{bmatrix} S_T \\ S_G \end{bmatrix} + \begin{bmatrix} 0 & 0 & \eta_{CHP,e} & 0 \\ 0 & \eta_{HP,h} & \eta_{CHP,h} & \eta_{GF,h} \\ 0 & 0 & 0 & 0 \end{bmatrix} \begin{bmatrix} S_{PtG} \\ S_{HP} \\ S_{CHP} \\ S_{GF} \end{bmatrix} - \begin{bmatrix} 0 & 0 \\ 1 & 0 \\ 0 & 1 \end{bmatrix} \begin{bmatrix} S^{in}_{HS} \\ S^{in}_{HS} \end{bmatrix} + \begin{bmatrix} 0 & 0 \\ 1 & 0 \\ 0 & 1 \end{bmatrix} \begin{bmatrix} S^{out}_{HS} \\ S^{out}_{GS} \end{bmatrix} \tag{1}$$

where $\eta_{T,e}$ is the energy transmission efficiency of the transformer; $\eta_{CHP,e}$ is the energy conversion efficiency from gas to electricity of the CHP unit; $\eta_{CHP,h}$ and $\eta_{GF,h}$ are the energy conversion efficiencies from gas to heat of the CHP unit and the gas furnace, respectively; and $\eta_{HP,h}$ is the energy conversion efficiency from electricity to heat of the heat pump.

Similarly, the relationship between state variables and input port variables is given as (2).

$$\begin{bmatrix} P_e \\ P_g \end{bmatrix} = \begin{bmatrix} 1 & 0 \\ 0 & 1 \end{bmatrix} \begin{bmatrix} S_T \\ S_G \end{bmatrix} + \begin{bmatrix} 1 & 1 & 0 & 0 \\ -\eta_{PtG,g} & 0 & 1 & 1 \end{bmatrix} \begin{bmatrix} S_{PtG} \\ S_{HP} \\ S_{CHP} \\ S_{GF} \end{bmatrix} \tag{2}$$

where $\eta_{PtG,g}$ is the conversion efficiency from electricity to methane of the PtG facility.

2.3. Integrated demand response

For an EH equipped with advanced metering infrastructure (AMI) and information communication technology (ICT), various IDR programs, e.g., price-based DR programs and incentive-based IDR programs, can be successfully implemented to improve the operation characteristic of the IRES. To formulate the customers' behaviors with respect to various DR programs, a general economic load model is presented in [30,31] to achieve the maximum benefit of the customers in electricity and gas consumption, and it is further employed in [32] to minimize the operation cost of an EH. In this paper, this widely accepted model is adopted to illustrate the price-based IDR program, and the modeling process with price elasticity is briefly described as follows.

The sensitivity of customers' energy demands with respect to different energy prices is usually described by the elasticity. If the customers' energy demands are only sensitive to the energy prices in the current period, these customers will only have a negative self-elasticity of energy demands. Conversely, if the customers' energy demands are sensitive to the energy prices in the other periods, these customers will have a positive cross-elasticity of energy demands. The self-elasticity and cross-elasticity are presented as [33]

$$E_{d,tt} = \frac{\rho^{ini}_{dt}}{L^{ini}_{dt}} \frac{\partial L_{dt}}{\partial \rho_{dt}},\ d \in \Omega_E \tag{3}$$

$$E_{d,t\tau} = \frac{\rho^{ini}_{d\tau}}{L^{ini}_{dt}} \frac{\partial L_{dt}}{\partial \rho_{d\tau}},\ t \neq \tau,\ d \in \Omega_E \tag{4}$$

where $\Omega_E = \{e,g,h\}$ is the set of different energy resources; $E_{d,tt}$ is the self-elasticity of load demand d at time t responsible to the energy price at time t, and its value is always negative; $E_{d,t\tau}$ is the cross-elasticity of load demand d at time t responsible to the energy price at time τ, and its value is always positive; L^{ini}_{dt} and L_{dt} are the initial energy consumption and modified energy consumption of load demand d at time t; ρ^{ini}_{dt} and ρ_{dt} are the initial energy price and modified energy price of load demand d at time t.

The customers' net benefit is equal to the difference between the obtained benefit from energy consumption and the energy purchasing cost.

$$B(L_{dt}) = \psi(L_{dt}) - \rho_{dt} L_{dt},\ d \in \Omega_E \tag{5}$$

For the modified energy consumption of customers, the widely adopted benefit function can be expressed as [34]

$$\psi(L_{dt}) = \psi(L^{ini}_{dt}) + \rho^{ini}_{dt}(L_{dt} - L^{ini}_{dt})\left(1 + \frac{L_{dt} - L^{ini}_{dt}}{2E_{d,tt}L^{ini}_{dt}}\right),\ d \in \Omega_E \tag{6}$$

To achieve the maximum of customers' net benefit, the differential equation $\partial B(L_{dt})/\partial L_{dt} = 0$ should be calculated, and then the customers' energy consumption can be formulated with the self-elasticity in the current period.

$$L_{dt} = L^{ini}_{dt}\left[1 + E_{d,tt}\left(\frac{\rho_{dt} - \rho^{ini}_{dt}}{\rho^{ini}_{dt}}\right)\right],\ d \in \Omega_E \tag{7}$$

Similarly, the customers' energy consumption with the cross-elasticity in the other periods can be expressed as

$$L_{dt} = L^{ini}_{dt}\left[1 + \sum_{\tau \in \Omega_T \& \tau \neq t} E_{d,t\tau}\left(\frac{\rho_{d\tau} - \rho^{ini}_{d\tau}}{\rho^{ini}_{d\tau}}\right)\right],\ d \in \Omega_E \tag{8}$$

Combining Eqs. (7) and (8), the customers' energy consumption under the maximum net benefit is represented as [30]

$$L_{dt} = L^{ini}_{dt}\left[1 + E_{d,tt}\left(\frac{\rho_{dt} - \rho^{ini}_{dt}}{\rho^{ini}_{dt}}\right) + \sum_{\tau \in \Omega_T \& \tau \neq t} E_{d,t\tau}\left(\frac{\rho_{d\tau} - \rho^{ini}_{d\tau}}{\rho^{ini}_{d\tau}}\right)\right],\ d \in \Omega_E \tag{9}$$

Note that the load response model in Eq. (9) is both suitable for the electricity load and gas load. Meanwhile, we assume that the heat load demand is inelastic in the EH, i.e., self-elasticity and cross-elasticity of heat load are equal to zero. Thus, the IDR program in the EH mainly includes the electricity demand response (EDR) and gas demand response (GDR).

3. EED model of the IRES

3.1. Gas emission modeling

To consider the environmental impacts on the IRES, the gas emissions from the combustion of fossil fuels cannot be neglected. As shown in Figs. 1 and 2, coal-fired units, gas-fired units and EHs (referring to CHP units and gas furnaces) are the main emission sources of CO_2, NOx and SO_2. CO_2 is one of the primary greenhouse gases, and its emission should be controlled to mitigate the global warming. Nowadays, various policies have been developed to reduce the CO_2 emission, such as carbon tax and carbon trading scheme. Compared with the simple

penalty by adding a carbon tax rate, emission quotas will be allocated to the CO_2 emission sources in the carbon trading scheme. According to the differences between actual emissions and emission quotas, the CO_2 emission sources can then choose to purchase or sell their emission quotas for emission permit or obtaining profit. In addition, NOx and SO_2 are typical air pollutants, which are harmful to the environment and human health. Thus, different air pollution control technologies have been applied to significantly reduce them. For instance, low NOx burner (LNB) and selective catalytic reduction (SCR) technology have been widely deployed in fossil-fired units to reduce the NOx emission, and the flue gas desulfurization (FGD) technology is adopted for reducing the SO_2 emission from the coal-fired units. Note that the SO_2 emission intensity of gas-fired units is negligible when it is compared with that of coal-fired units, and more than 90% SO_2 from the flue gas of coal-fired units can be absorbed by the FGD technology. Therefore, the gas emissions of the IRES only focus on the CO_2 and NOx in this paper.

3.1.1. CO_2 emission and quota

For the coal-fired units and gas-fired units, the CO_2 emissions are proportional to their power outputs (10) and (11).

$$Q_i^{CO_2} = \mu_i^{CO_2} P_i,\ i \in \Omega_{CU} \tag{10}$$

$$Q_j^{CO_2} = \mu_j^{CO_2} P_j,\ j \in \Omega_{GU} \tag{11}$$

where P_i and P_j are the power outputs of the coal-fired unit i and the gas-fired unit j, respectively; $Q_i^{CO_2}$ and $Q_j^{CO_2}$ are the CO_2 emissions of the coal-fired unit i and the gas-fired unit j, respectively; $\mu_i^{CO_2}$ and $\mu_j^{CO_2}$ are the CO_2 emission coefficients of the coal-fired unit i and the gas-fired unit j, respectively.

Similarly, the CO_2 emissions from CHP units and gas furnaces are proportional to their power outputs and heat supplies. Note that P2G facilities in EHs can reduce the CO_2 emission of CHP units by synthesizing natural gas, thus the net CO_2 emission from an EH can be described as

$$Q_k^{CO_2} = \mu_{CHP,k}^{CO_2} P_{\overline{CHP},k} + \mu_{GF,k}^{CO_2} S_{GF,k}\eta_{GF,k} - \upsilon_{PtG,k}^{CO_2} S_{PtG,k},\ k \in \Omega_{EH} \tag{12}$$

where $Q_k^{CO_2}$ is the net CO_2 emission of the EH k; $\mu_{CHP,k}^{CO_2}$ and $\mu_{GF,k}^{CO_2}$ are the CO_2 emission coefficients of the CHP unit and the gas furnace in the EH k, respectively; $\upsilon_{PtG,k}^{CO_2}$ is the CO_2 reaction coefficient of the PtG facility in the EH k; $P_{\overline{CHP},k}$ is the equivalent power output of the CHP unit in the EH k, and it can be expressed as

$$P_{\overline{CHP},k} = S_{CHP,k}(\eta_{CHP,e,k} + \xi_{h,e}\eta_{CHP,h,k}),\ k \in \Omega_{EH} \tag{13}$$

where $\xi_{h,e}$ is the conversion rate from heat to electric power of CHP units.

In the carbon trading scheme, the CO_2 emission quotas of coal-fired units, gas-fired units and EHs are allocated as in (14)–(16) [13].

$$Q_{R,i}^{CO_2} = \chi_e^{CO_2} P_i,\ i \in \Omega_{CU} \tag{14}$$

$$Q_{R,j}^{CO_2} = \chi_e^{CO_2} P_j,\ j \in \Omega_{GU} \tag{15}$$

$$Q_{R,k}^{CO_2} = \chi_e^{CO_2} P_{\overline{CHP},k} + \chi_h^{CO_2} S_{GF,k}\eta_{GF,k},\ k \in \Omega_{EH} \tag{16}$$

where $\chi_e^{CO_2}$ and $\chi_h^{CO_2}$ are the CO_2 emission quotas of unit electric power and unit heat, respectively.

3.1.2. NOx emission

The operation status of the SCR facility is related to the power outputs of both coal-fired units and gas-fired units, and the SCR will have to be shut down if the power output of a deployed unit is lower than a certain threshold. Additionally, when the power output of a combined cycle gas turbine (CCGT) is less than a critical value, the lean premixed combustion mode of the CCGT will be switched to the diffusive combustion mode to maintain the combustion stability, which can significantly increase the NOx emission. Therefore, after deploying the LNB and the SCR, the NOx emissions from coal-fired units and gas-fired units (referring to CCGT units) can be described as different segmental functions (17), (18) [5], respectively.

$$Q_i^{NO_x} = \begin{cases} \kappa_i^{NO_x}\delta_i^{NO_x}(\alpha_i^{NO_x}P_i^2 + \beta_i^{NO_x}P_i + \gamma_i^{NO_x}),\ \lambda_i^{NO_x}P_{i,max} \leqslant P_i \leqslant P_{i,max} \\ \delta_i^{NO_x}(\alpha_i^{NO_x}P_i^2 + \beta_i^{NO_x}P_i + \gamma_i^{NO_x}),\ P_{i,min} \leqslant P_i \leqslant \lambda_i^{NO_x}P_{i,max} \end{cases},\ i \in \Omega_{CU} \tag{17}$$

where $\alpha_i^{NO_x}$, $\beta_i^{NO_x}$, and $\gamma_i^{NO_x}$ are the NOx emission coefficients of the coal-fired unit i; $\delta_i^{NO_x}$ and $\kappa_i^{NO_x}$ are the NOx emission reduction coefficients of the coal-fired unit i equipped with the LNB and the SCR, respectively; $\lambda_i^{NO_x}$ is the threshold coefficient to distinguish the operation status of the SCR in the coal-fired unit i. If the power output P_i is larger than $\lambda_i^{NO_x}P_{i,max}$, the SCR will be started up; otherwise, the SCR will be shut down.

$$Q_j^{NO_x} = \begin{cases} \kappa_j^{NO_x}\delta_j^{NO_x}(\mu_{L,j}^{NO_x}P_j),\ \varsigma_j^{NO_x}P_{j,max} \leqslant P_j \leqslant P_{j,max} \\ \kappa_j^{NO_x}\delta_j^{NO_x}(\mu_{D,j}^{NO_x}P_j),\ \lambda_j^{NO_x}P_{j,max} \leqslant P_j \leqslant \varsigma_j^{NO_x}P_{j,max} \\ \delta_j^{NO_x}(\mu_{D,j}^{NO_x}P_j),\ P_{j,min} \leqslant P_j \leqslant \lambda_j^{NO_x}P_{j,max} \end{cases},\ j \in \Omega_{GU} \tag{18}$$

where $\mu_{L,j}^{NO_x}$ and $\mu_{D,j}^{NO_x}$ are the NOx emission coefficients of the gas-fired unit i in the lean premixed combustion mode and diffusive combustion mode, respectively; $\delta_j^{NO_x}$ and $\kappa_j^{NO_x}$ are the NOx emission reduction coefficients for the gas-fired unit i equipped with the LNB and the SCR, respectively; $\lambda_j^{NO_x}$ is the threshold coefficient to distinguish the operation status of the SCR in the gas-fired unit j, and its value is nearly 0.5; $\varsigma_j^{NO_x}$ is the combustion mode switching coefficient of gas-fired unit j, and its value is often chosen between 0.65 and 0.7.

For the EH, Eq. (18) is also suitable for the CHP unit, and the NOx emission of the gas furnace is considered proportionally to its heat supply.

$$Q_k^{NO_x} = \sum_{k\in\Omega_{EH}} (Q_{CHP,k}^{NO_x} + \mu_{GF,k}^{NO_x} S_{GF,k}\eta_{GF,k}),\ k \in \Omega_{EH} \tag{19}$$

where $Q_{CHP,k}^{NO_x}$ is the NOx emission from the CHP unit in EH k by replacing P_j in (18) by $P_{\overline{CHP},k}$; $\mu_{GF,k}^{NO_x}$ is the NOx emission coefficient of the gas furnace in EH k.

3.2. Objective function

The objective function of proposed EED model is to minimize the total cost of the IRES (20), which is the sum of operation cost F_{oc} and emission cost F_{ec}.

$$\min F = F_{oc} + F_{ec} \tag{20}$$

The operation cost (21) includes the fuel cost of coal-fired units, production cost of gas wells, and operation cost of EHs. The fuel consumption of the coal-fired unit is determined by its heat rate curve (22), while the operation cost of the EH (23) is composed of the P2G facility cost, heat storage cost, and gas storage cost.

$$F_{oc} = \sum_{t\in\Omega_T}\left[\sum_{i\in\Omega_{CU}}\rho_i G(P_{it}) + \sum_{\omega\in\Omega_{GW}}\rho_\omega Q_{\omega t} + \sum_{k\in\Omega_{EH}} C_{kt}\right] \tag{21}$$

$$G(P_{it}) = a_i P_{it}^2 + b_i P_i + c_i \tag{22}$$

$$C_{kt} = \rho_{PtG,k}S_{PtG,kt} + \rho_{HS,k}S_{HS,kt}^{out} + \rho_{GS,k}S_{GS,kt}^{out} \tag{23}$$

The emission cost (24) includes the carbon trading cost and NOx emission penalty cost. The carbon trading cost is proportional to the carbon trading price and the difference between CO_2 emission and CO_2 emission quota. The NOx emission penalty cost is calculated by the emission amount and emission penalty price.

$$F_{ec} = \sum_{t\in\Omega_T} [\rho^{CO_2}(Q_t^{CO_2} - Q_{R,t}^{CO_2}) + \rho^{NO_x} Q_t^{NO_x}] \tag{24}$$

where the CO_2 emission $Q_t^{CO_2}$, CO_2 emission quota $Q_{R,t}^{CO_2}$, and NOx emission $Q_t^{NO_x}$ at time t can be expressed as

$$Q_t^{CO_2} = \sum_{i\in\Omega_{CU}} Q_{it}^{CO_2} + \sum_{j\in\Omega_{GU}} Q_{jt}^{CO_2} + \sum_{k\in\Omega_{EH}} Q_{kt}^{CO_2} \tag{25}$$

$$Q_{R,t}^{CO_2} = \sum_{i\in\Omega_{CU}} Q_{R,it}^{CO_2} + \sum_{j\in\Omega_{GU}} Q_{R,jt}^{CO_2} + \sum_{k\in\Omega_{EH}} Q_{R,kt}^{CO_2} \tag{26}$$

$$Q_t^{NO_x} = \sum_{i\in\Omega_{CU}} Q_{it}^{NO_x} + \sum_{j\in\Omega_{GU}} Q_{jt}^{NO_x} + \sum_{k\in\Omega_{EH}} Q_{kt}^{NO_x} \tag{27}$$

3.3. Constraints

In addition to the constraints (1)–(19), other constraints for the EED model of the IRES are given as follows.

3.3.1. Power system constraints

For the power transmission network, since the line resistance is much less than the line reactance, the DC power flow is usually adopted to focus on the real power. At each bus, the net nodal power injection, i.e., the difference between the power supply and the load demand, is equal to the sum of real power flow of transmission lines connected to this bus.

$$\sum_{i\in\Omega_{CU}} A_{bi}P_{it} + \sum_{j\in\Omega_{GU}} A_{bj}P_{jt} + \sum_{w\in\Omega_{WF}} A_{bw}P_{wt} - \sum_{k\in\Omega_{EH}} A_{bk}P_{e,kt} - EL_{bt} = \sum_{l\in\Omega_{TL}} A_{bl}PL_{lt},\ b\in\Omega_B \tag{28}$$

The power outputs of coal-fired units and gas-fired units are limited by their minimum loads, maximum capacities, and ramp rates, respectively.

$$\begin{cases} P_{i,\min} \leqslant P_{it} \leqslant P_{i,\max} \\ RD_i \leqslant P_{it} - P_{i,t-1} \leqslant RU_i \end{cases},\ i\in\Omega_{CU} \tag{29}$$

$$\begin{cases} P_{j,\min} \leqslant P_{jt} \leqslant P_{j,\max} \\ RD_j \leqslant P_{jt} - P_{j,t-1} \leqslant RU_j \end{cases},\ j\in\Omega_{GU} \tag{30}$$

Assuming that the wind power can be accurately forecasted, then the power outputs of wind farms should be less than their forecasting values.

$$0 \leqslant P_{wt} \leqslant P_{wt}^f,\ w\in\Omega_{WF} \tag{31}$$

The real power flow in each transmission line is calculated by the line impedance and the difference of bus voltage angles.

$$PL_{lt} = (\theta_{l1} - \theta_{l2})/x_l,\ l\in\Omega_{TL} \tag{32}$$

The real power flow in each transmission line and the voltage angle at each bus cannot exceed their lower and upper bounds. Meanwhile, a reference bus should be given to calculate the voltage angles of other buses.

$$\begin{cases} PL_{l,\min} \leqslant PL_{lt} \leqslant PL_{l,\max},\ l\in\Omega_{TL} \\ \theta_{b,\min} \leqslant \theta_{bt} \leqslant \theta_{b,\max},\ b\in\Omega_B \\ \theta_{ref} = 0 \end{cases} \tag{33}$$

3.3.2. Natural gas system constraints

The natural gas system is composed of gas wells, pipelines, compressors, and consumers. This paper assumes that the gas flow characteristics will not change at each dispatch period, and the natural gas system constraints are considered under the steady-state mathematical model. Similarly to the nodal power balance, the total gas flow injection at each node should be equal to the total gas flow withdrawn, which can be described as

$$\sum_{\omega\in\Omega_{GW}} B_{n\omega}Q_{\omega t} - \sum_{j\in\Omega_{GU}} B_{nj}Q_{jt} - \sum_{k\in\Omega_{EH}} B_{nk}P_{g,kt} - GL_{nt} = \sum_{p\in\Omega_{GP}} B_{np}Q_{pt},\ n\in\Omega_N \tag{34}$$

where the gas consumption of a gas-fired unit can be calculated by its heat rate curve and higher heating value (HHV).

$$Q_{jt} = G(P_{jt})/\mathrm{HHV},\ j\in\Omega_{GU} \tag{35}$$

The natural gas from gas suppliers are mainly transported to consumers through pipelines. According to whether the compressors are deployed or not, the natural gas pipelines are classified as passive pipelines (without compressors) and active pipelines (with compressors). For a passive pipeline, the relationship between the gas flow and node pressures is widely described by the Weymouth Eq. (36), in which the gas flow is transported from the high pressure node to the low pressure node (37).

$$Q_{pt} = \mathrm{sgn}(Pr_{p1,t}, Pr_{p2,t})C_p\sqrt{|Pr_{p1,t}^2 - Pr_{p2,t}^2|},\ p\in\Omega_{PP} \tag{36}$$

$$\mathrm{sgn}(Pr_{p1,t}, Pr_{p2,t}) = \begin{cases} +1, & Pr_{p1,t} \geqslant Pr_{p2,t} \\ -1, & Pr_{p1,t} < Pr_{p2,t} \end{cases} \tag{37}$$

Since the pressure loss will be caused by the pipeline resistance during the gas flow transmission process, the compressors are deployed at active pipelines to maintain the desired pressure levels of the natural gas system. For an active pipeline, the pressure relationship between the incoming node and the outcoming node can be expressed as [35]

$$\sigma_{c,\min}Pr_{c1,t} \leqslant Pr_{p2,t} \leqslant \sigma_{c,\max}Pr_{c1,t},\ c\in\Omega_{COM} \tag{38}$$

Additionally, the gas well outputs and the nodal pressures should be limited by their lower and upper bounds.

$$Q_{\omega,\min} \leqslant Q_{\omega t} \leqslant Q_{\omega,\max},\ \omega\in\Omega_{GW} \tag{39}$$

$$Pr_{n,\min} \leqslant Pr_{nt} \leqslant Pr_{n,\max},\ n\in\Omega_N \tag{40}$$

3.3.3. EH constraints

Since EHs are the electricity load and gas load of the regional energy supply systems, the input electricity and input gas of each EH should be nonnegative (41) and (42).

$$P_{e,kt} \geqslant 0 \tag{41}$$

$$P_{g,kt} \geqslant 0 \tag{42}$$

According to the relationship of input port variables and state variables, the transmission limits of transformers and gas pipelines can be described as (43) and (44).

$$0 \leqslant S_{T,kt} \leqslant P_{e,kt} \tag{43}$$

$$0 \leqslant S_{G,kt} \leqslant P_{g,kt} + S_{PtG,kt}\eta_{PtG,k} - P_{CHP,k,\min}\eta_{CHP,k} - Q_{GF,k,\min} \tag{44}$$

For the energy conversion elements, the input energy limits of heat pump and gas furnaces are determined by their capacities (45) and (46), and the input powers of P2G facilities are related to the electrolysis technologies (47). For example, the minimal partial load should be at least 20% of rated capacity for the alkaline water electrolysis technology, and it can be as low as 5% of rated capacity for the proton exchange membrane electrolysis technology [36]. Additionally, the electric power output limits and the ramp constraints of CHP units are expressed as (48) and (49), respectively.

$$P_{HP,k,\min} \leqslant S_{HP,kt} \leqslant P_{HP,k,\max} \tag{45}$$

$$Q_{GF,k,\min} \leqslant S_{GF,kt} \leqslant Q_{GF,k,\max} \tag{46}$$

$$I_{PtG,kt}P_{PtG,k,\min} \leqslant S_{PtG,kt} \leqslant I_{PtG,kt}P_{PtG,k,\max} \tag{47}$$

$$P_{\mathrm{CHP},k,\min} \leqslant S_{\mathrm{CHP},kt}\eta_{\mathrm{CHP,e},k} \leqslant P_{\mathrm{CHP},k,\max} \tag{48}$$

$$\begin{cases} (S_{\mathrm{CHP},kt} - S_{\mathrm{CHP},k,t-1})\eta_{\mathrm{CHP,e},k} \leqslant RU_{\mathrm{CHP},k} \\ (S_{\mathrm{CHP},k,t-1} - S_{\mathrm{CHP},kt})\eta_{\mathrm{CHP,e},k} \leqslant RD_{\mathrm{CHP},k} \end{cases} \tag{49}$$

Compared to the electric energy, the heat and gas can be easily stored in large quantities through existing technologies. The heat storage facility constraints and gas storage facility constraints both include the storage capacity limits, injection and withdrawal rate limits, and operation status limits, which are similarly shown in (50) and (51), respectively.

$$\begin{cases} ES_{\mathrm{HS},kt} = ES_{\mathrm{HS},k,t-1} + S^{\mathrm{in}}_{\mathrm{HS},kt}\eta^{\mathrm{in}}_{\mathrm{HS},k} - S^{\mathrm{out}}_{\mathrm{HS},kt}/\eta^{\mathrm{out}}_{\mathrm{HS},k} \\ ES_{\mathrm{HS},k,\min} \leqslant ES_{\mathrm{HS},kt} \leqslant ES_{\mathrm{HS},k,\max} \\ I^{\mathrm{in}}_{\mathrm{HS},kt}Q^{\mathrm{in}}_{\mathrm{HS},k,\min} \leqslant S^{\mathrm{in}}_{\mathrm{HS},kt} \leqslant I^{\mathrm{in}}_{\mathrm{HS},kt}Q^{\mathrm{in}}_{\mathrm{HS},k,\max} \\ I^{\mathrm{out}}_{\mathrm{HS},kt}Q^{\mathrm{out}}_{\mathrm{HS},k,\min} \leqslant S^{\mathrm{out}}_{\mathrm{HS},kt} \leqslant I^{\mathrm{out}}_{\mathrm{HS},kt}Q^{\mathrm{out}}_{\mathrm{HS},k,\max} \\ \sum_{t\in\Omega_{\mathrm{T}}}(S^{\mathrm{in}}_{\mathrm{HS},kt}\eta^{\mathrm{in}}_{\mathrm{HS},k} - S^{\mathrm{out}}_{\mathrm{HS},kt}/\eta^{\mathrm{out}}_{\mathrm{HS},k}) = 0 \\ I^{\mathrm{in}}_{\mathrm{HS},kt} + I^{\mathrm{out}}_{\mathrm{HS},kt} \leqslant 1 \end{cases} \tag{50}$$

$$\begin{cases} ES_{\mathrm{GS},kt} = ES_{\mathrm{GS},k,t-1} + S^{\mathrm{in}}_{\mathrm{GS},kt}\eta^{\mathrm{in}}_{\mathrm{GS},k} - S^{\mathrm{out}}_{\mathrm{GS},kt}/\eta^{\mathrm{out}}_{\mathrm{GS},k} \\ ES_{\mathrm{GS},k,\min} \leqslant ES_{\mathrm{GS},kt} \leqslant ES_{\mathrm{GS},k,\max} \\ I^{\mathrm{in}}_{\mathrm{GS},kt}Q^{\mathrm{in}}_{\mathrm{GS},k,\min} \leqslant S^{\mathrm{in}}_{\mathrm{GS},kt} \leqslant I^{\mathrm{in}}_{\mathrm{GS},kt}Q^{\mathrm{in}}_{\mathrm{GS},k,\max} \\ I^{\mathrm{out}}_{\mathrm{GS},kt}Q^{\mathrm{out}}_{\mathrm{GS},k,\min} \leqslant S^{\mathrm{out}}_{\mathrm{GS},kt} \leqslant I^{\mathrm{out}}_{\mathrm{GS},kt}Q^{\mathrm{out}}_{\mathrm{GS},k,\max} \\ \sum_{t\in\Omega_{\mathrm{T}}}(S^{\mathrm{in}}_{\mathrm{GS},kt}\eta^{\mathrm{in}}_{\mathrm{GS},k} - S^{\mathrm{out}}_{\mathrm{GS},kt}/\eta^{\mathrm{out}}_{\mathrm{GS},k}) = 0 \\ I^{\mathrm{in}}_{\mathrm{GS},kt} + I^{\mathrm{out}}_{\mathrm{GS},kt} \leqslant 1 \end{cases} \tag{51}$$

For the IDR in the EH, to guide the energy consumption of consumers, the prices of different energy resources can be specified in an acceptable range (52). Meanwhile, according to the price changes of different energy resources, only some consumers will actively change their energy consumption patterns (53). Additionally, to maintain the customers' comfort and also for the simplicity of calculation, the total energy consumption for each type of energy resource is assumed to be the same as its original energy consumption pattern (54).

$$\phi^{\mathrm{l}}_d\rho^{\mathrm{ini}}_d \leqslant \rho_{dt} \leqslant \phi^{\mathrm{u}}_d\rho^{\mathrm{ini}}_d,\ d \in \Omega_{\mathrm{E}} \tag{52}$$

$$\varphi^{\mathrm{l}}_d L^{\mathrm{ini}}_d \leqslant L_{dt} \leqslant \varphi^{\mathrm{u}}_d L^{\mathrm{ini}}_d,\ d \in \Omega_{\mathrm{E}} \tag{53}$$

$$\sum_{t\in\Omega_{\mathrm{T}}} L_{dt} = \sum_{t\in\Omega_{\mathrm{T}}} L^{\mathrm{ini}}_d,\ d \in \Omega_{\mathrm{E}} \tag{54}$$

where ϕ^{l}_d and ϕ^{u}_d are the acceptable price adjustment coefficients of load demand d; φ^{l}_d and φ^{u}_d are the IDR participation coefficients of load demand d.

3.4. Linearization of equations

The proposed environmental economic dispatch model is a non-convex mixed-integer nonlinear programming (MINLP), and it is often difficult to solve directly. Therefore, nonlinear Eqs. (17), (18), (22) and (36) are linearized by piecewise linearization methods [37,38], and then the presented model is converted into a mixed-integer linear programming (MILP), which can be solved by fast and high efficient optimization tools, such as CPLEX and Gurobi. The corresponding description is presented in Appendix A.

4. Case study

An integrated 6-bus power system and 6-node natural gas system, an integrated IEEE 39-bus power system and 20-node Belgian natural gas system, and an integrated IEEE 118-bus power system and 40-node natural gas system are adopted to illustrate the effectiveness of the proposed model. The presented model is coded in MATLAB aided by YALMIP with CPLEX 12.6, and all case studies are implemented on a PC with Inter (R) Core (TM) i7-6700 CPU (3.4 GHz) and 8 GB RAM.

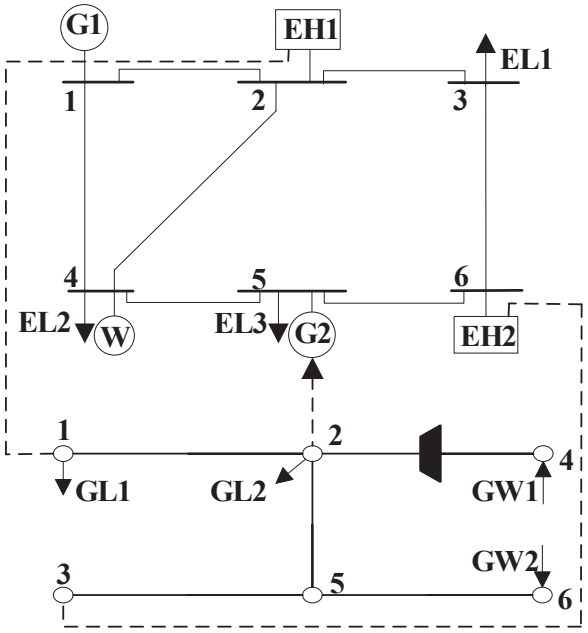

Fig. 3. 6-bus power system and 6-node natural gas system.

4.1. 6-bus power system and 6-node natural gas system

The 6-bus power system and 6-node natural gas system are shown in Fig. 3. The 6-bus power system consists of one coal-fired unit G1, one gas-fired unit G2, one wind farm, and three electricity loads EL1-EL3. The 6-node natural gas system includes two gas wells GW1-GW2, one compressor, five pipelines, and two gas loads GL1-GL2. Two EHs with the same structure as in Fig. 2 are depicted as EH1 and EH2. Parameters of generators, gas wells, EHs, transmission lines, and pipelines are referred to [24,25]. In the two EHs, the elasticities of electricity load and gas load are obtained from [39]. The acceptable price adjustment coefficients are set as $\phi^{\mathrm{l}}_d = 0.8$ and $\phi^{\mathrm{u}}_d = 1.2$, and the IDR participation coefficients are set as $\varphi^{\mathrm{l}}_d = 0.8$ and $\varphi^{\mathrm{u}}_d = 1.2$. G1, G2 and CHP units in the two EHs are equipped with both LNB and SCR, and the corresponding parameters can be found in [5]. Parameters of carbon trading are the same as in [13]. The load profiles of each EH are depicted in Fig. 4 with maximum electricity load 184.32 MW, maximum gas load 2260.01 kcf,

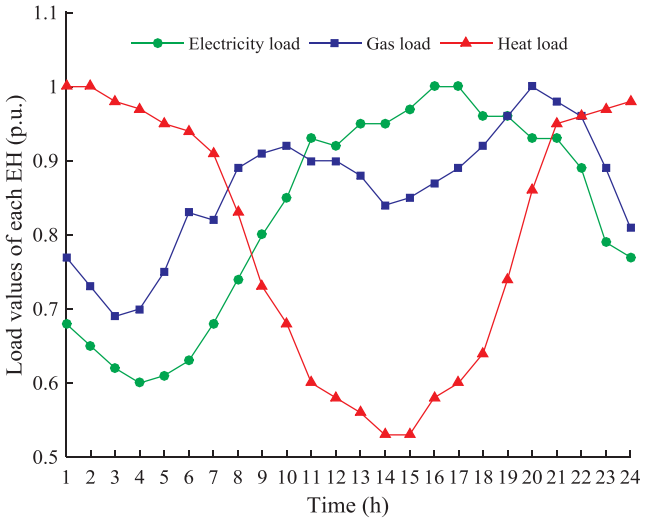

Fig. 4. Load profiles of each EH.

and maximum heat load 1035.81 MBtu. In addition to the two EHs, the forecasted values of electricity load, gas load and wind power are shown in Fig. 5 with peak values of 307.2 MW, 6780 kcf, and 185.33 MW, respectively.

The following seven cases are considered.

Case 0: Economic dispatch of IRES without EHs.
Case 1: Economic dispatch of IRES.
Case 2: EED of IRES considering the emission cost of NOx and CO_2.
Case 3: Case 1 considering the EDR in EHs.
Case 4: Case 1 considering the GDR in EHs.
Case 5: Case 1 considering the IDR in EHs.
Case 6: Case 2 considering the IDR in EHs.

4.1.1. Results and analysis of the seven cases

The main contribution of this manuscript is to study the impacts of the carbon trading scheme, air pollution control technologies, and IDR program on the operation characteristics of the presented IRES. Thus, Case 1 performs the base case to validate the effectiveness of the presented model. Compared with previously published papers [10,11,16,19,20], the main difference in Case 1 is that EHs are introduced to represent the connections between the regional transmission networks and the loads. To prove the merits of the applied approach, a similar case in [10] is considered as Case 0 through removing the two EHs from the IRES in Case 1, and the heat loads in original EHs are replaced by equivalent gas loads. The analysis and the corresponding results are given as follows.

In Case 0, the wind power, coal-fired unit G1, and gas well GW1 have the priority to be selected to supply electricity load and gas load, due to their cheaper operation cost, while the gas-fired unit G2 and gas well GW2 are mainly used to supply the remaining electricity load and gas load. After introducing the EHs in Case 1, the CHP units with higher efficiency are utilized to generate the electricity and heat. Meanwhile, the heat pumps, gas furnaces, heat storage facilities, and gas storage facilities are also cooperated to minimize the operation cost of IRES. Though an operation cost of $5435.2 is spent by the EHs, the total operation cost in Case 1 can save $19488.06 compared with that in Case 0. Additionally, the comparison results for the power output of gas-fired unit G2 and gas production of gas well GW2 in Cases 0–1 are shown in Fig. 6. The energy supplies from the gas-fired unit G2 and gas well GW2 are dramatically decreased most of the time. This also demonstrates that the operational characteristics of the presented IRES in Case 1 has been improved considerably.

Considering the presented IRES, the cost results of Cases 1–6 are shown in Table 1. In Case 1, the generation cost of gas-fired unit G2 is larger than coal-fired unit G1, and the power outputs of CHP units are limited by both electricity load demand and heat load demand. Therefore, in addition to the wind farm, electricity load demand is mainly supplied by the coal-fired unit G1. Both the operation cost and emission cost are considered in Case 2, and thus a compromise between them should be achieved. However, the emission cost $17284.49 is very small compared with the operation cost $598324.64 in Case 2, which causes only a slight increase of the operation cost compared with Case 1. Moreover, the load profiles of electricity load and gas load are optimized by the EDR in Case 3 and the GDR in Case 4, and thus more operation costs can be saved than that in Case 1. In Cases 5–6, the corresponding operation and emission costs are lower than those in Cases 1–4 due to the application of the IDR.

To analyze the influence of different DR programs (i.e., EDR, GDR, and IDR) on EHs, the electricity load profiles and gas load profiles of EHs are shown in Figs. 7 and 8, respectively. The comparison for peak values and valley values of electricity load and gas load in Case 1 and Cases 3–5 is presented in Table 2. Compared with Case 1, both electricity load profiles and gas load profile are optimized with smaller peak-valley differences in Case 3. However, the peak values of gas load in Cases 4–5 are slightly higher than that in Case 1. To explain it in more details, the comparison results of operation costs in Case 1 and Cases 3–5 are presented in Table 3.

As shown in Table 3, to meet the larger variations of electricity load and gas load in Case 1, more heat energy is injected into and also withdrawn from the heat storage facilities, which results in larger heat storage cost than those in Cases 3–5. In addition, Fig. 4 depicts the gas load and heat load that will reach their peak values alternatively in hours 20–24. During these time periods, the gas load in EH1 cannot be completely satisfied in Case 1, due to the natural gas pipeline congestion between node 1 and node 2. To meet the gas load demand, the P2G facility in EH1 has to be started to synthesize natural gas, and thus extra electricity will be consumed. In Case 3, the EDR program can improve the electricity load profile, and the CHP units with higher efficiency will be utilized to meet more electricity load demand and heat load demand. Therefore, the operation costs of coal-fired units, gas wells, and heat storage facilities are less than those in Case 1. However, since the natural gas demand in hours 20–24 is still high, partial gas load in EH1 should be supplied by the PtG facility in EH1 to compromise the natural gas pipeline congestion. After implementing the GDR program in Cases 4–5, the gas load of EH2 will be increased in hours 20–24, which can avoid the pipeline congestion by improving the nodal pressures of the natural gas system. Especially in Case 5, both the electricity load profile and gas load profile are improved under the IDR program, the operation costs of coal-fired units, heat storage facilities, and gas storage facilities are reduced considerably. However, with more gas consumption for the CHP units, the production cost of gas wells in Case 5 is slightly higher than that in Case 1, and Cases 3–4.

To further analyze the emission cost, the gas emission results of NOx and CO_2 are also calculated in Case 1, and the corresponding results of Case 1 and Case 6 are presented in Tables 4 and 5. In Case 1, the main role of the gas-fired unit G2 is to supply the electricity load peak, while the power output of gas-fired unit G2 always equals the lower limit value in Case 6, due to the optimized load profiles by implementing the IDR. Additionally, to reduce the emissions of NOx and CO_2 in Case 6, the power output of coal-fired unit G1 will be curtailed 280.1 MWh, and two gas furnaces (GF1 and GF2) will reduce the heat supply 994.93 MBtu. Instead, more electricity load demand and heat load demand will be supplied by CHP units with higher efficiency. Therefore, the NOx emission is reduced by 68.32 kg compared with Case 1, and the differences between the CO_2 emission and CO_2 emission quota is reduced to 946.63 tons from 1084.43 tons in Case 1.

4.1.2. Sensitivity analysis

The operation status of the EED of IRES is sensitive to the electricity

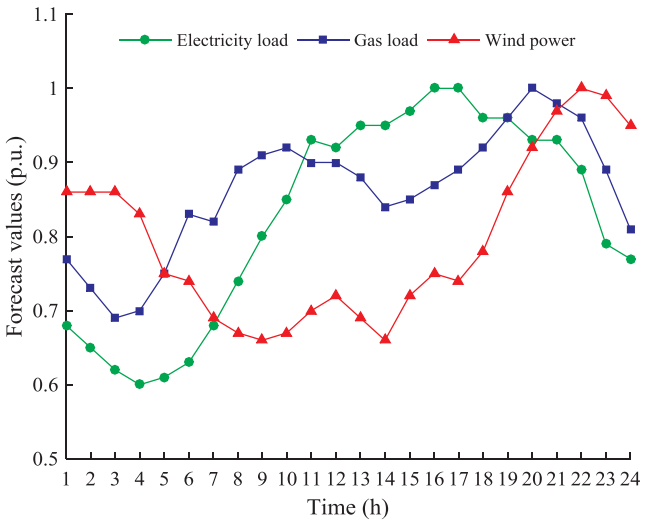

Fig. 5. Forecasted values of electricity load, gas load, and wind power.

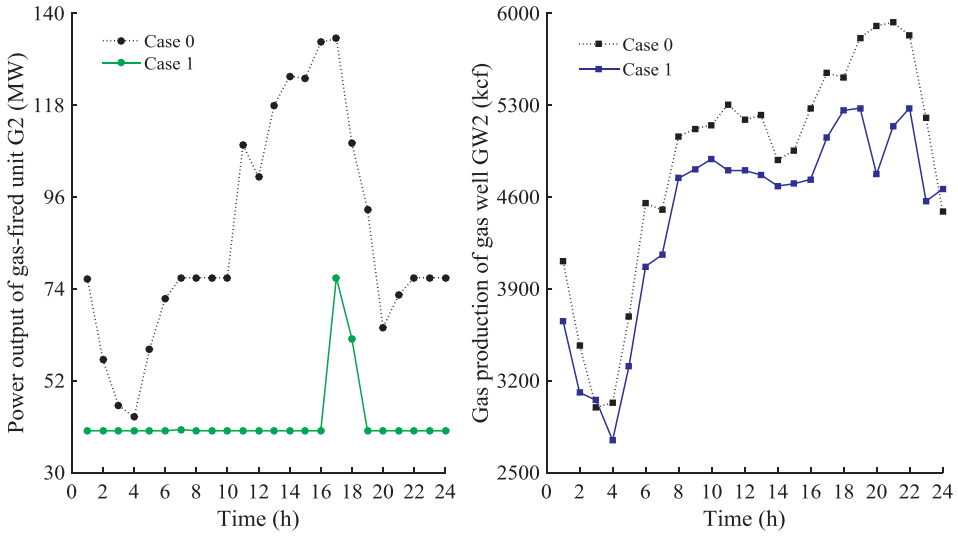

Fig. 6. Comparisons of power outputs of G2 and gas production of GW2 in Cases 0–1.

Table 1
Cost results of Cases 1–6.

	Total cost ($)	Operation cost ($)	Emission cost ($)
Case 1	598,228.59	598,228.59	0
Case 2	615,609.13	598,324.64	17,284.49
Case 3	593,509.67	593,509.67	0
Case 4	589,152.14	589,152.14	0
Case 5	587,784.40	587,784.40	0
Case 6	603,170.68	587,936.87	15,233.81

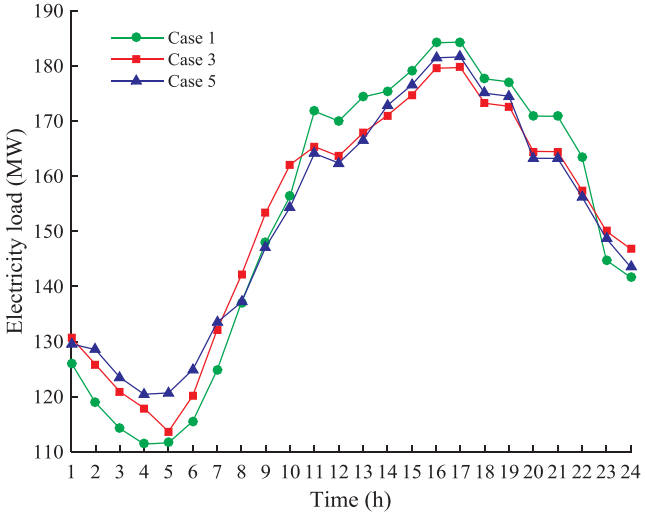

Fig. 7. Electricity load profiles of EHs in Case 1, Case 3, and Case 5.

price, gas price, wind power penetration, NOx emission penalty price and carbon trading price. To discuss these influencing factors in the proposed model, Case 6 is set as the base scenario 1, and its parameters ρ_{dt}^{ini}, P_{wt}^{f}, ρ^{NO_x}, and ρ^{CO_2} are set as the reference values. In this paper, eleven scenarios for each influencing factor are considered, and the related parameters in each scenario can be calculated by the scenario number and the reference values in the base scenario 1.

(1) Electricity price scenarios: $\phi_{SN,\text{e}}^{\text{l}} = 1 - 0.1 \times (SN - 1)$ and $\phi_{SN,\text{e}}^{\text{l}} + \phi_{SN,\text{e}}^{\text{u}} = 2$.

(2) Gas price scenarios: $\phi_{SN,\text{g}}^{\text{l}} = 1 - 0.1 \times (SN - 1)$ and $\phi_{SN,\text{g}}^{\text{l}} + \phi_{SN,\text{g}}^{\text{u}} = 2$.

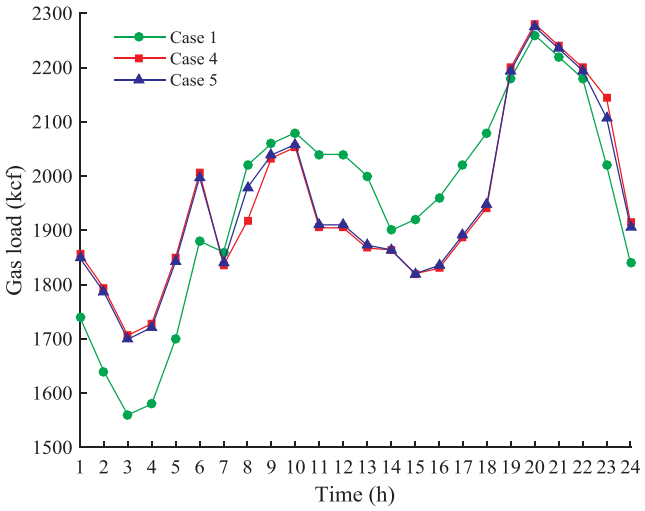

Fig. 8. Gas load profiles of EHs in Case 1, Case 4, and Case 5.

Table 2
Peak values and valley values of electricity load and gas load in Case 1 and Cases 3–5.

	Peak values		Valley values	
	Electricity load (MW)	Gas load (kcf)	Electricity load (MW)	Gas load (kcf)
Case 1	184.32	2260.01	111.41	1560
Case 3	179.71	2260.01	113.69	1560
Case 4	184.32	2280.57	111.41	1706.34
Case 5	181.62	2275.26	120.44	1699.35

Table 3
Comparison for operation costs in Case 1 and Cases 3–5.

	Coal-fired unit cost ($)	Gas well cost ($)	P2G cost ($)	HS cost ($)	GS cost ($)
Case 1	117,286.91	475,506.49	3006.41	728.11	1700.67
Case 3	114,397.73	475,356.47	1435.27	619.54	1700.67
Case 4	112,226.38	475,274.35	0	463.91	1187.50
Case 5	110,426.62	475,996.97	0	410.81	950

Table 4
Total power outputs of generators, CHPs and GFs in Case 1 and Case 6.

	G1 (MWh)	G2 (MWh)	CHP1 (MWh)	CHP2 (MWh)	GF1 (MBtu)	GF2 (MBtu)
Case 1	4004.9	1019.01	2757.95	2177.39	494.43	500.5
Case 6	3724.8	960.32	3086.37	2186.84	203.57	338.21

Table 5
Gas emission results in Case 1 and Case 6.

	NOx emission (kg)	CO_2 emission (ton)	CO_2 emission quota (ton)
Case 1	710.84	8367.51	7283.08
Case 6	642.52	8177.84	7231.21

(3) Wind power penetration scenarios: $P^{f}_{SN,wt} = [1 + 0.1 \times (SN - 1)]P^{f}_{wt}$.

(4) NOx emission penalty price scenarios: $\rho^{NO_x}_{SN} = [1 + (SN - 1)]\rho^{NO_x}$.

(5) Carbon trading price scenarios: $\rho^{CO_2}_{SN} = [1 + (SN - 1)]\rho^{CO_2}$.where SN is the scenario number of each influencing factor, and it is equal to an integer ranging from 1 to 11; $(\cdot)_{SN}$ is the parameter value under the scenario SN. The total costs of the IRES under different scenarios are shown in Fig. 9.

With the increase of electricity price, gas price and wind power penetration, the total cost of the IRES will decrease monotonously. Similarly, along with the increase of NOx emission penalty price and carbon trading price, the total cost of IRES will increase monotonously. More detailed results of operation costs and environment costs are shown in Figs. 10–14.

As shown in Figs. 10 and 11, both the operation cost and emission cost become higher with the increase of electricity price and gas price. However, if the gas price is equal to zero, the natural gas pipelines will still be congested with the increase of electricity price. To meet the gas load demand in these scenarios, energy storage facilities are used more frequently, and the P2G facility in EH1 has to covert electricity into synthetic natural gas. Conversely, if the gas price is larger than zero, enough natural gas can be supplied smoothly to meet all gas load demand. With the increase of gas price, more electricity and heat will be provided by CHP units, which will result in more NOx emissions in these scenarios.

In Fig. 12, since the operational cost of wind power is very low and considered zero here, wind power should be utilized as much as possible. With the increase of wind power penetration, the power outputs of generators G1–G2 and CHP units will be reduced, while the heat pumps, gas furnaces and heat storage facilities will be used more frequently to meet the heat load demand. The emissions of NOx and CO_2 will drastically decrease, since the emissions from gas furnaces are less than those from generators and CHP units. However, NOx emission is related to the threshold value of SCR device and the combustion mode of CCGT. When the wind power penetration is larger than 1.7 times of reference value, the lower power outputs of coal-fired units, gas-fired units and CHP units cause more SCR devices being stopped. Meanwhile, the gas-fired units and CHP units will switch to higher diffusive combustion mode. Therefore, the emission cost will increase due to the higher NOx emission.

As shown in Fig. 13, when the NOx emission penalty price is less than 5 times of the reference value or more than 8 times of the reference value, the NOx emission penalty cost has almost no effect on the operation cost, and the emission costs will increase in proportion to the NOx emission penalty price. However, when the NOx emission penalty price is equal to 6 or 7 times of the reference value, the power outputs of coal-fired units and CHP units will increase at certain time to reduce the NOx emission by starting the SCR devices. Thus, the operation cost has a significant increase in these scenarios. In Fig. 14, with the increase of carbon trading price, the power outputs of coal-fired units will be reduced due to their higher CO_2 emission intensity, and the high efficient CHP units will provide more electricity energy and heat energy. Since the natural gas is more expensive than coal, the operation cost is slowly increasing. When the carbon trading price is more than 9 times of the reference value, the P2G facilities are started to capture CO_2 from the CHP units, which will result in a sudden increase of the operation cost.

4.2. IEEE 39-bus power system and Belgium 20-node natural gas system

The modified IEEE 39-bus power system includes seven coal-fired units, two wind farms, forty-six branches, and twenty-one electricity loads, and the original three gas-fired units of power system are replaced by three EHs. The Belgium 20-node natural gas system is composed of two gas wells, three active pipelines equipped with compressors, twenty-one passive pipelines, and nine gas loads. Three EHs are connected to the buses 30, 36, 37 of power system, and nodes 5, 8, 14 of natural gas system, respectively. The structures of the three EHs are the same as Fig. 2. The profiles of forecasted electricity load, gas load and wind power are the same as Fig. 5, and the corresponding peak values of forecasted electricity load, gas load and wind power are 4718.08 MW, 132761.2 kcf, and 1530.81 MW, respectively. Case 1 and Case 6 in Section 4.1 are considered in this test system.

Case 1: Similar to Fig. 5, hours 1–7 are the valley period of electricity load, and the heat loads are close to their peak values. Except for wind power, the power outputs of coal-fired units and gas-fired units are near to their minimum outputs, and the remaining electricity load are provided by CHP units due to their high efficiency. However, limited by the fixed electrothermal ratio of CHP units, part of the heat load needs to be supplied by heat pumps and gas furnaces. In the daytime, the electricity load is larger than its valley period, and the heat load is less than their peak values. Thus heat pumps and gas furnaces will be shut down, and the heat loads are supplied by CHP units. To meet the peak period of heat load, surplus heat energy from CHP units is injected into the heat storage facilities. Additionally, the wind power is much

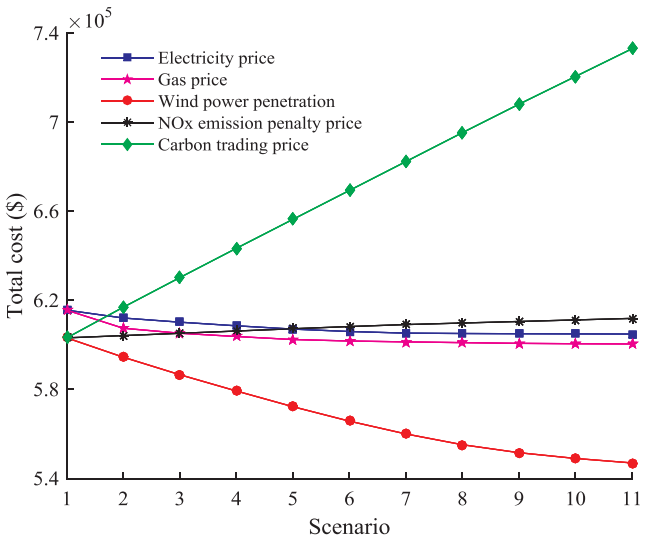

Fig. 9. Total costs under different scenarios.

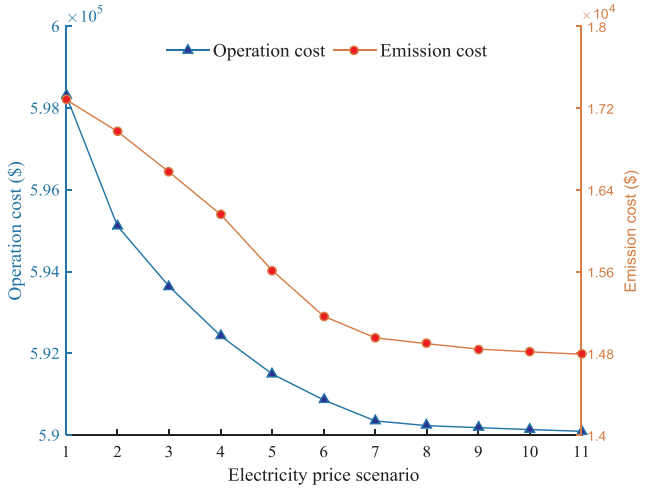

Fig. 10. Operation costs and emission costs under different electricity price scenarios.

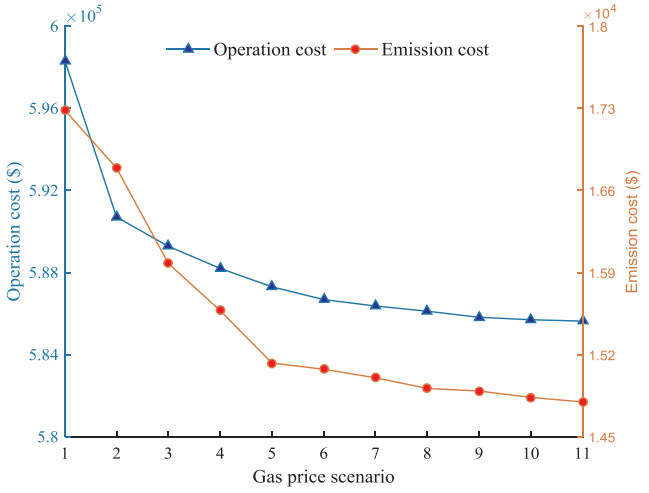

Fig. 11. Operation costs and emission costs under different gas price scenarios.

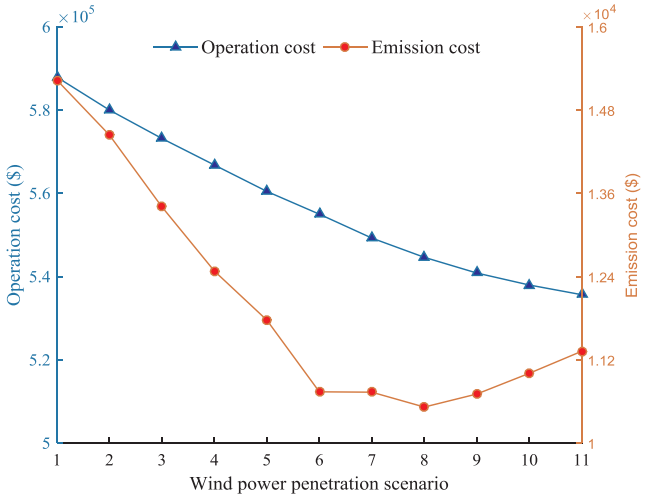

Fig. 12. Operation costs and emission costs under different wind power penetration scenarios.

lower than its peak value, and thus the electricity load is mainly supplied by coal-fired units. At night, the wind power, gas load and heat load are close to their peak values. To meet the gas load demand, the

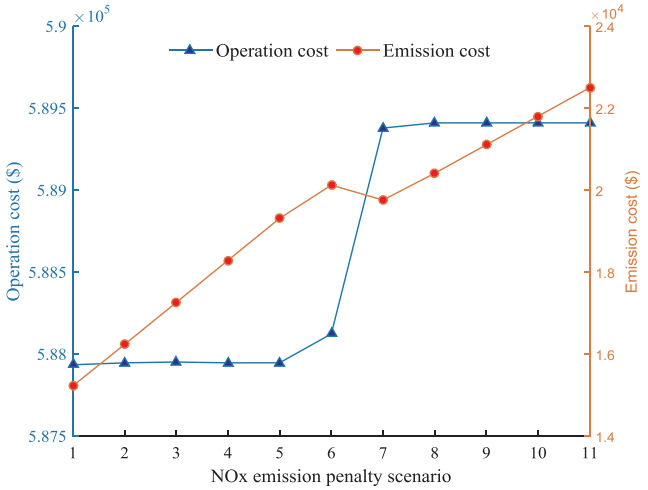

Fig. 13. Operation costs and emission costs under different NOx emission penalty price scenarios.

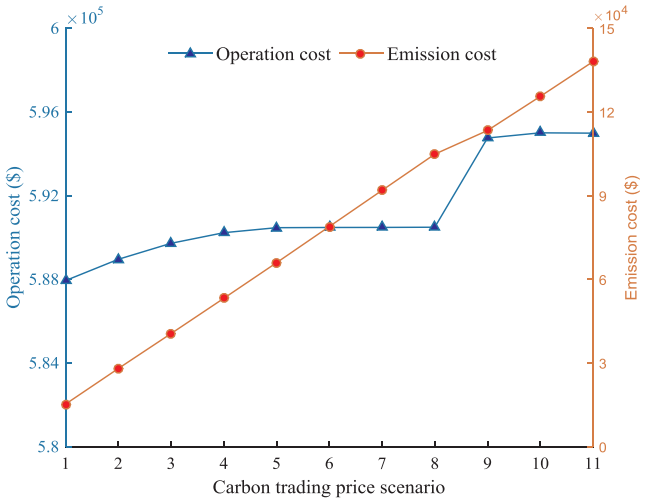

Fig. 14. Operation costs and emission costs under different carbon trading price scenarios.

gas consumption of CHP units will be reduced, and the heat load is mainly supplied by the heat storage facilities, heat pumps and gas furnaces. Meanwhile, the power outputs of coal-fired units will be reduced to utilize the wind power. However, the electricity load decreases rapidly from hour 22 to hour 23, which results in the wind power curtailment 385.05 MWh due to the ramp down limits of coal-fired units.

Case 6: In this case, the load peak-valley differences of electricity load and gas load are reduced by the IDR, and the wind power can be utilized completely. Compared with coal-fired units and gas-fired units, CHP units can reduce the operation cost and CO_2 emission simultaneously, and thus more electricity energy and heat energy are produced by CHP units. Since the heat load demand is the same as Case 1, the amount of energy converted by heat pumps and gas furnaces is reduced, and the heat storage facilities are mainly used to coordinate with the CHP units. To maintain the gas supply of CHP units and other gas load, more natural gas is injected into, and also withdrawn from, the gas storage facilities. In addition, the emission cost is considered in Case 6, and thus both the NOx emission and carbon trading costs are less than those in Case 1. The comparison results of the two cases are shown in Table 6. Compared with Case 1, the operation cost can reduce nearly 16.99% in Case 6. Meanwhile, the NOx emission can reduce 27.14%, and 2382.89 ton CO_2 can be avoided to be purchased from the carbon

Table 6
Comparison results of two cases.

	Operation cost ($)	NOx emission (kg)	CO_2 emission (ton)	CO_2 emission quota (ton)
Case 1	40,285,404.28	44,261.07	157,209.80	125,218.43
Case 6	33,442,112.73	32,250.15	156,412.72	126,803.84

trading market in Case 6.

4.3. IEEE 118-bus power system and 40-node natural gas system

A large-scale test IRES, i.e., the modified IEEE 118-bus power system and a 40-node natural gas system, is used to further validate the effectiveness of the proposed model. The modified IEEE 118-bus power system has 32 coal-fired units (7766.2 MW), 6 gas-fired units (600 MW), 6 CHP units (1800 MW), 10 wind farms (3000 MW), and 186 transmission lines. The 40-node natural gas system is composed of two Belgium 20-node natural gas systems as described in Section 4.2, which are connected by the node 4 and node 40. Two network topologies can be found in [40]. The 6 CHP units are extended to 6 EHs as in Fig. 2, and their detailed locations are the buses 40, 42, 56, 91, 92, 113 and the nodes 16, 20, 25, 36, 40, 5. Parameters of other internal elements in the 6 EHs are multiplied by different factors to match the installed CHP units. Similarly, Case 1 and Case 6 in Section 4.1 are considered in this large test system.

Since the emission cost and the IDR are both integrated in Case 6, $38649.91 additional operation cost savings and 34090.51 kg NOx additional emission reduction can be achieved compared with Case 1. However, limited by the operation characteristics of the SCR and the combustion modes of gas-fired units, coal-fired units and gas-fired units will have to increase their power outputs to reduce the NOx emission in Case 6, which results in extra 87.60 ton CO_2 emission than that in Case 1. Fortunately, the load profiles of 6 EHs are improved by the IDR in Case 6, and more loads are supplied by the CHP units with higher efficiency. Therefore, 147.13 ton CO_2 emission quota is saved in Case 6 compared with Case 1.

To further validate the feasibility of the presented solution method for a large system, the stochastic optimization method in [28] is adopted to consider the impact of wind power uncertainty to the integrated IEEE 118-bus power system and 40-node natural gas system. Firstly, we assume that the hourly wind power forecast error follows a normal distribution function with zero mean and 15% standard deviation. Then 2000 initial scenarios of wind power are generated through the Monte Carlo (MC) simulation. Since the computation time of the presented model will increase with the numbers of scenarios, the 2000 initial scenarios are reduced to 5 by the SCENRED tool in the General Algebraic Modeling System (GAMS) to find a tradeoff between the accuracy and the computation burden. After that, the stochastic optimization model is calculated by combining the five wind power scenarios and the corresponding probabilities.

The expected total cost of the stochastic optimization model is $19544650.81, which is $149676.89 less than the deterministic optimization model. Meanwhile, compared with the computational time of 325.70 s for the deterministic optimization in Case 6, the computational time of the stochastic optimization model will increase to 1702.63 s. These results demonstrate that the presented solution method is acceptable for the day-ahead emission economic dispatch of a large size IRES.

5. Conclusion

This paper proposes an environmental economic dispatch model for the coordinated operation of integrated regional energy system, which is composed of the electricity and natural gas supplying networks and energy hubs. To reduce the greenhouse gas CO_2 and air pollutant NOx, the carbon trading scheme and air pollutant control technologies are introduced, and the corresponding carbon trading cost and NOx emission penalty cost are added as the emission cost of the integrated regional energy system. Furthermore, a price-based integrated demand response is embedded into the energy hub for further analyzing its impact on the environmental economic dispatch of the integrated energy system. Simulation results show that the integrated demand response program can optimize the electricity and gas load profiles with smaller variations, which contributes to the increased wind power utilization and reduced economic operational cost of the integrated regional energy system. The proposed environmental economic dispatch model can reduce the NOx emission and avoid purchasing part CO_2 emission quota. Furthermore, according to the sensitivity analysis of different scenarios, the total cost of the presented model changes monotonously against five influence factors. However, the changes of operation cost and emission cost are more complex due to various reasons, such as shutting down of selective catalytic reduction devices or starting up of power to gas facilities. Since this paper focuses on the deterministic model of integrated regional energy system with steady-state constraints, as an immediate future task, dynamic gas flow model and district heating network constraints will be investigated along with various uncertainties. Meanwhile, preserving privacy among different energy sectors (gas, electricity, etc.) will be further studied by considering limited information exchanges.

Declaration of Competing Interest

The authors declared that there is no conflict of interest.

Acknowledgement

This paper is financially supported by the National Natural Science Foundation of China (No. 61873225) and (No. 61374098); Provincial Graduate Innovation Assistant Project 2018 (No. 023000307); and the Natural Science Foundation of Hebei Province (No. F2016203507).

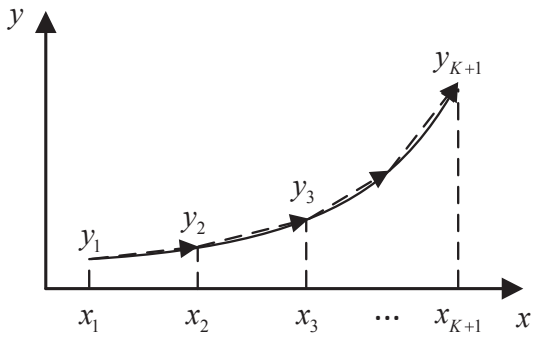

Fig. 15. Piecewise linearization of quadratic equations.

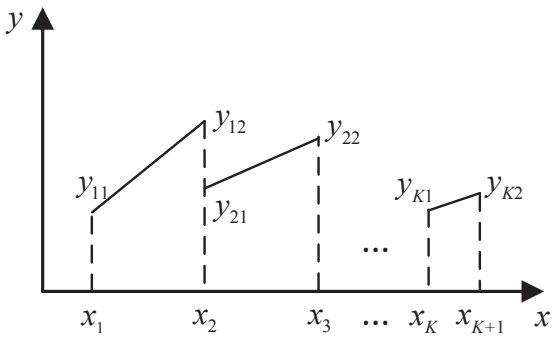

Fig. 16. Piecewise linearization of segmental equations.

Appendix A

A.1. Linearization method 1

To convert the proposed MINLP model into a MILP model, the nonlinear gas flow Eq. (36) is rewritten as (55) by replacing the $Pr^2_{p1,t}$ and $Pr^2_{p2,t}$ by $Prs_{p1,t}$ and $Prs_{p2,t}$. After that, only the nonlinear term $Q_{pt}\ |Q_{pt}|$ should be linearized by considering its functional form $y = x\ |x|$. Meanwhile, the NOx emission in Eq. (17) and the heat rate curves in Eq. (22) can be described by a quadratic function $y = \varepsilon_1 x^2 + \varepsilon_2 x + \varepsilon_3$.

$$Q_{pt}\ |Q_{pt}| = C_p^2 (Prs_{p1,t} - Prs_{p2,t}),\ p \in \Omega_{PP} \tag{55}$$

To linearize these univariate quadratic functions (17), (22), and (55), the incremental piecewise linearization method [37] is adopted due to its advantages in terms of computational speed. As shown in Fig. 15, the quadratic function curve is approximated by K straight lines. With the coordinate values at both ends of K straight lines, the values of linearized function y and variable x are calculated by (56) and (57), respectively. In (58) and (59), ϑ_k is a continuous variable for the portion of straight line k, and ℓ_k is a binary variable to force the so-called filling conditions, i.e., if the variable x is located at straight line $k + 1$, then $\ell_k = 1$, $\vartheta_h = 1 (1 \leqslant h \leqslant k)$, and $0 \leqslant \vartheta_{k+1} \leqslant 1$.

$$y = y_1 + \sum_{k \in \Omega_K} (y_{k+1} - y_k)\vartheta_k \tag{56}$$

$$x = x_1 + \sum_{k \in \Omega_K} (x_{k+1} - x_k)\vartheta_k \tag{57}$$

$$0 \leqslant \vartheta_k \leqslant 1,\ k \in \Omega_K \tag{58}$$

$$\vartheta_{k+1} \leqslant \ell_k \leqslant \vartheta_k,\ 1 \leqslant k \leqslant K \tag{59}$$

A.2. Linearization method 2

After the linearization of NOx emission in Eq. (17), the emission characteristics of Eqs. (17) and (18) can depicted as in Fig. 16. With the coordinate values at both ends of each segment, (60)–(63) can further convert these segmental equations into the corresponding linear formulations [38]. The values of linearized function y and variable $\times$ are calculated by (60), (61), respectively. In (62), (63), o_{k1} and o_{k2} are the continuous variables to determine the location of segment k, and ν_k is a binary variable to limit the variable and function locating at a single segment.

$$y = \sum_{k \in \Omega_K} (o_{k1} y_{k1} + o_{k2} y_{k2}) \tag{60}$$

$$x = \sum_{k \in \Omega_K} (o_{k1} x_k + o_{k2} x_{k+1}) \tag{61}$$

$$0 \leqslant o_{k1} \leqslant 1,\ 0 \leqslant o_{k2} \leqslant 1,\ k \in \Omega_K \tag{62}$$

$$o_{k1} + o_{k2} = \nu_k,\ \sum_{k \in \Omega_K} \nu_k = 1 \tag{63}$$

References

[1] Paris agreement. [Online]. Available: http://www.htemp.com/detail/16876.html; 2015 [accessed on 4 Jul. 2019].

[2] Omer A. Power, people and pollutions. Renew Sust Energ Rev Sep. 2008;12(7):1864–89.

[3] EIA. Monthly energy review. [Online]. Available: http://www.eia.gov/totalenergy/data/monthly/#naturalgas/; 2019 [accessed on 6 Jul. 2019].

[4] Lu Z, Feng T, Li X. Low-carbon emission/economic power dispatch using the multi-objective bacterial colony chemotaxis optimization algorithm considering carbon capture power plant. Int J Elect Power Energy Syst 2013;53:106–12.

[5] Geng Z, Chen Q, Xia Q, Kirschen DS, Kang C. Environmental generation scheduling considering air pollution control technologies and weather effects. IEEE Trans Power Syst Jan. 2017;32(1):127–36.

[6] GWEC. Global wind power report [Online]. Available: https://gwec.net/members-area-market-intelligence/reports/; 2018 [accessed on 6 Jul. 2019].

[7] Ding Y, Shao C, Yan J, Song Y, Zhang C, Guo C. Economical flexibility options for integrating fluctuating wind energy in power systems: the case of China. Appl Energy Oct. 2018;228:426–36.

[8] Lu Z, He S, Feng T, Li X, Guo X, Sun X. Robust economic/emission dispatch considering wind power uncertainties and flexible operation of carbon capture and storage. Int. J. Elect. Power Energy Syst Dec. 2014;63:285–92.

[9] Wu J, Yan J, Jia H, Hatziargyriou N, Djilali N, Sun H. Integrated energy systems.

Appl Energy 2016;167:155–7.
[10] Alabdulwahab A, Abusorrah A, Zhang X, Shahidehpour M. Coordination of interdependent natural gas and electricity infrastructures for firming the variability of wind energy in stochastic day-ahead scheduling. IEEE Trans Sustain Energy 2015;6(2):606–15.
[11] He L, Lu Z, Zhang J, Geng L, Zhao H, Li X. Low-carbon economic dispatch for electricity and natural gas systems considering carbon capture systems and power-to-gas. Appl Energy Aug. 2018;224:357–70.
[12] Jiang T, Deng H, Bai L, Zhang R, Li X, Chen H. Optimal energy flow and nodal energy pricing in carbon emission-embedded integrated energy systems. CSEE JPES 2018;4(2):179–87.
[13] Qu K, Yu T, Huang L, Yang B, Zhang X. Decentralized optimal multi-energy flow of large-scale integrated energy systems in a carbon trading market. Energy 2018;149:779–91.
[14] Cheng Y, Zhang N, Wang Y, Yang J, Kang C, Xia Q. Modeling carbon emission flow in multiple energy systems. IEEE Trans Smart Grid Jul. 2019;10(4):3562–74.
[15] Su Y, Nie W, Zhou Y, Tan M, Qiao H. An interval based cost-emissions optimization strategy for electricity-gas-heat integrated energy systems under uncertainty and demand response. Beijing, China: in Proc. EI2; 2017.
[16] Qu K, Shi S, Yu T, Wang W. A convex decentralized optimization for environmental-economic power and gas system considering diversifed emission control. Appl Energy 2019;240:630–45.
[17] Zhang N, Hu Z, Dai D, Dang S, Yao M, Zhou Y. Unit commitment model in smart grid environment considering carbon emissions trading. IEEE Trans Smart Grid 2016;7(1):420–7.
[18] Li X, Zhang R, Bai L, Li G, Jiang T, Chen H. Stochastic low-carbon scheduling with carbon capture power plants and coupon-based demand response. Appl Energy 2018;210:1219–28.
[19] Cui H, Li F, Hu Q, Bai L, Fang X. Day-ahead coordinated operation of utility-scale electricity and natural gas networks considering demand response based virtual power plants. Appl Energy 2016;176:183–95.
[20] Zhang X, Shahidehpour M, Alabdulwahab A, Abusorrah A. Hourly electricity demand response in the stochastic day-ahead scheduling of coordinated electricity and natural gas networks. IEEE Trans Power Syst 2016;31(1):592–601.
[21] He C, Zhang X, Liu T, Wu L. Distributionally robust scheduling of integrated gas-electricity systems with demand response. IEEE Trans Power Syst 2019. https://doi.org/10.1109/TPWRS.2019.2907170. [in press].
[22] Bai L, Li F, Cui H, Jiang T, Sun H, Zhu J. Interval optimization based operating strategy for gas-electricity integrated energy systems considering demand response and wind uncertainty. Appl Energy 2016;167:270–9.
[23] Wang J, Zhong H, Ma Z, Xia Q, Kang C. Review and prospect of integrated demand response in the multi-energy system. Appl Energy 2017;202:772–82.
[24] Zhang Y, He Y, Yan M, Guo C, Ding Yi. Linearized stochastic scheduling of interconnected energy hubs considering integrated demand response and wind uncertainty. Energies 2018;11(9).
[25] Ni L, Liu W, Wen F, Xue Y, Dong Z, Zheng Y, Zhang Rui. Optimal operation of electricity, natural gas and heat systems considering integrated demand responses and diversified storage devices. J Mod Power Syst Clean Energy 2018;6(3):423–37.
[26] Bahrami S, Sheikhi A. From demand response in smart grid toward integrated demand response in smart energy hub. IEEE Trans Smart Grid 2016;7(2):650–8.
[27] Yan M, He Y, Shahidehpour M, Ai X, Li Z, Wen J. Coordinated regional-district operation of integrated energy systems for resilience enhancement in natural disasters. IEEE Trans Smart Grid 2019. https://doi.org/10.1109/TSG.2018.2870358. [in press].
[28] Li Y, Zou Y, Tan Y, Cao Y, Liu X, Shahidehpour M, et al. Optimal stochastic operation of integrated low-carbon electric power, natural gas, and heat delivery system. IEEE Trans Sustain Energy 2018;9(1):273–83.
[29] Shao C, Wang X, Shahidehpour M, Wang X, Wang B. An MILP-based optimal power flow in multicarrier energy systems. IEEE Trans Sustain Energy 2017;8(1):239–48.
[30] Aalami HA, Parsa Moghaddam M, Yousefi GR. Demand response modeling considering interruptible/curtailable loads and capacity market programs. Appl. Energy, Jan. 2010;87(1):243–50.
[31] Li L, Gong C, Wang D, Zhu K. Multi-agent simulation of the time-of-use pricing policy in an urban natural gas pipeline network: A case study of Zhengzhou. Energy 2013;52:37–43.
[32] Aghamohamadi M, Hajiabadi ME, Samadi M. A novel approach to multi energy system operation in response to DR programs; an application to incentive-based and time-based schemes. Energy 2018;156:534–47.
[33] Kirschen DS. Demand-side view of electricity markets. IEEE Trans Power Syst 2003;18(2):520–7.
[34] Schweppe FC, Caramanis MC, Tabors RD, Bohn RE. Spot pricing of electricity. Boston, MA: Kluwer Ltd.; 1989.
[35] Tomasgard A, Rømo F, Fodstad M, Midthun K. Optimization models for the natural gas value chain. Geom Model Numer Simul Optimiz 2007:521–58.
[36] Gotz M, Lefebvre J, Mors F, Koch AM, Graf F, Bajohr S, et al. Renewable Power-to-Gas: A technological and economic review. Renew Energy 2016;85:1371–90.
[37] Correa-Posada C, Sánchez-Martín P. Integrated power and natural gas model for energy adequacy in short-term operation. IEEE Trans Power Syst 2015;30(6):3347–55.
[38] Geng Z, Conejo AJ, Chen Q, Kang C. Power generation scheduling considering stochastic emission limits. Int. J Elect Power Energy Syst 2018;95:374–83.
[39] Zhang Y, et al. Optimal dispatch of integrated electricity-natural gas system considering demand response and dynamic natural gas flow. Auto. Electric Power Syst. 2018;42(20):1–8.
[40] Liu F, Bie Z, Wang X. Day-ahead dispatch of integrated electricity and natural gas system considering reserve scheduling and renewable uncertainties. IEEE Trans Sustain Energy 2019;10(2):646–58.